Astron. Astrophys. 140, 185–198

ASTRONOMY AND ASTROPHYSICS

Properties of solar magnetic fluxtubes as revealed by Fe I lines

S. K. Solanki and J. O. Stenflo

Institute of Astronomy, ETH-Zentrum, CH-8092 Zürich, Switzerland

Received April 9, accepted July 2, 1984

Summary. The information contents in the solar spectrum for modelling of magnetic fluxtubes is explored by analysing the statistical properties of the Stokes I and V line profiles of 400 unblended Fe I lines. Methods of determining the temperature structure, photospheric magnetic field strength, magnetic filling factor, and microturbulence velocity are presented and used to provide estimates of these quantities in enhanced network and plage regions. Analysis of the magnetic line broadening shows that the magnetic field strength is approximately equal in network and plage regions, consistent with previous results. On the other hand, the temperature structures of the plage fluxtubes and the network elements are observed to be substantially different. Thus network fluxtubes are hotter in their lower layers as compared with plages. The variation of the Stokes V line asymmetries with line strength are found to be similar in the different solar regions, indicating similar velocity structures in plages and network elements. Empirical Landé factors for a number of Fe I lines suspected to deviate from LS coupling are also given.

Key words: solar magnetic fields – fluxtubes – Fe I – active regions – network – Landé factors

1. Introduction

In the decade following the discovery that both the quiet network and active region plages have approximately the same photospheric field strengths (Frazier and Stenflo, 1972), in the range of 1–2 kG (Stenflo, 1973), a number of models have been proposed describing the photospheric network, the plages, or the magnetic structure underlying both these phenomena, the fluxtube. These have been theoretical in nature (e.g. Spruit, 1976; Unno and Ribes, 1979; Ribes and Semel, 1980; Deinzer et al., 1982; Osherovich et al., 1983), or empirical (e.g. Shine and Linsky, 1974; Stenflo, 1975; Koutchmy and Stellmacher, 1978; Frazier and Stenflo, 1978; Chapman, 1977, 1979; Stellmacher and Wiehr, 1979).

Many different approaches have been tried. Among the empirical models Shine and Linsky (1974) used the damping wings of the Ca II K line to determine the temperature and pressure structure of a plage. This approach gives no information on the magnetic field strength and results in only an averaged plane-parallel model of the properties of the magnetic and non-magnetic regions, since even the best possible spatial resolution is at present too low to allow us to resolve the individual flux elements. If the filling factor of the magnetic elements is smaller than 0.5, as is the case for most faculae and is certainly so in the quiet region network, the spectrum is dominated by light coming from the non-magnetic regions. This is a general handicap for all models based on the analysis of unpolarized data, for example the plage models of Chapman (1977, 1979), which rely on fitting the profiles of eight weak to moderately strong lines.

A second class of models use polarization data to determine the properties of the fluxtubes alone. Examples of this approach are the universal (network and plage) model of Stenflo (1975) using the Stokes I and V profiles of the 5250.2 Å and 5247.1 Å lines of Fe I together with the line ratio technique (Stenflo, 1973), the plage model of Frazier and Stenflo (1978) using similar data, and the network model of Koutchmy and Stellmacher (1978) using the right and left circularly polarized profiles of the three iron lines 5567 Å, 6301.5 Å, and 6302.5 Å with high spatial resolution. All these models are based on the observations of a few lines and therefore depend critically on the details of their formation. They also suffer the disadvantage that the effects of temperature structure, velocity fields, and the magnetic inhibition of turbulence (Gough and Taylor, 1966) cannot be separated very well. The model of Koutchmy and Stellmacher further only gives averaged information on these properties, since the individual polarization profiles include light from non-magnetic regions as well, and only their difference, Stokes V, refers to the magnetic features alone.

The use of the Kitt Peak FTS as a polarimeter has given us the possibility of investigating the I and V profiles of hundreds of spectral lines observed simultaneously, allowing us to use a statistical approach to gain information from the polarization data. We have thus made ourselves independent of the spatial resolution used, as well as of any uncertainties pertaining to individual lines. With this method strong magnetic fields can be measured directly by their line broadening effects, independent of model parameters. It has also become possible to partially separate temperature, velocity, and turbulence effects, allowing us to set some constraints on fluxtube properties.

2. Observational data and reduction procedure

2.1. Observations

The observations which form the basis of the present paper were made on April 29–30, 1979 at the Kitt Peak McMath telescope, using the FTS adapted to record both intensity and polarization spectra simultaneously. Details of the technique used can be found in Brault (1978). Five recordings of different features near disk

Send offprint requests to: J. O. Stenflo

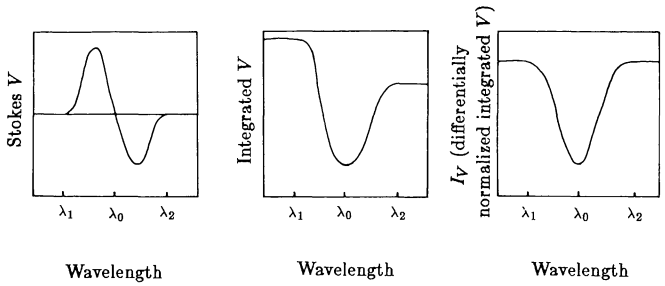

Fig. 1. Illustration of the transformation of a Stokes V profile into an I_V profile (Stokes I of the light from the fluxtube) using Eq. (2.4). Left: asymmetric V profile of a spectral line. λ_0 is the zero crossing wavelength, λ_1 and λ_2 are the integration boundaries. Center: integrated V profile (before differential renormalization). Right: I_V profile, i.e., integrated V after differential renormalization such that the continuum appears at a single level (see text)

center were made, ranging from the quiet sun network to strong plages. The five spectra corresponding to these features cover a wavelength range of over 1000 Å each, and have a spectral resolution of between 360,000 and 500,000, which means that the solar spectrum can be regarded as fully resolved. The spatial resolution is defined by a circular diaphragm of 10 arc s diameter. However, this has little to do with the "effective resolution", since the recorded polarization comes exclusively from sub-arc s magnetic elements covering only a small fraction of the 10 arc s aperture. Further details concerning the observational data can be found in Stenflo et al. (1984).

2.2. Data reduction

The great number of fully resolved line profiles contained in the FTS spectra provide us with an impressively rich source of information on fluxtubes and their surroundings. Since the information from magnetic features is concentrated in the Stokes V profiles, while the observed Stokes I profiles are mainly representative of the non-magnetic surrounding, we need to find a simple relation between V and I, to be able to use differentiable line profile effects to bring out the difference between the magnetic and non-magnetic atmospheres without having to rely on sophisticated radiative-transfer calculations. Such a relationship was introduced by Stenflo et al. (1984):

$$V=\sum_{n=0}^{\infty}\frac{1}{(2n+1)!}\frac{\partial^{2n+1}I_V}{\partial\lambda^{2n+1}}(\Delta\lambda_H)^{2n+1}, \tag{2.1}$$

where

$$\Delta\lambda_H=4.67\,10^{-13}g\lambda^2B \tag{2.2}$$

is the Zeeman splitting (with λ and $\Delta\lambda_H$ in Å, B in G). We have used the notation I_V for the intensity profile in (2.1), to stress that it refers to the same magnetic area from which the observed V originates. Thus we avoid confusion with the observed Stokes I, which has its largest contributions outside the "V areas". B in (2.2) is the intrinsic field strength in the "V areas", not the average over the resolution element. If the spectral line has an anomalous Zeeman splitting pattern, g in (2.2) has to be replaced by the effective Landé factor g_{eff}.

For a weak magnetic field, i.e. when the Zeeman splitting is much smaller than the line width, the higher order terms in (2.1) may be neglected and that expression simplifies to

$$V=\Delta\lambda_H\frac{\partial I_V}{\partial\lambda}. \tag{2.3}$$

Stenflo et al. (1984) also showed that the weak field approximation is valid on the sun, even in the presence of kG fields, for broad lines or for lines with a small Landé factor. By integrating (2.3) it is possible to determine the intensity profile that corresponds to a given V profile:

$$\frac{I_c-I_V}{I_c}=-\frac{1}{\Delta\lambda_H}\int_{\lambda_1}^{\lambda}\frac{V(\lambda')}{I_c}d\lambda', \tag{2.4}$$

where I_c is the intensity of the continuum and λ_1 is the lower integration boundary, chosen to be sufficiently far in the blue wing for V to approach zero (Fig. 1).

The intensity profile thus obtained contains only contributions from the fluxtube atmosphere (V being small, where the magnetic field is small). In this relatively simple manner the intensity spectrum produced inside the fluxtube can be determined (at least as a first order approximation), and it becomes possible to use techniques developed for the interpretation of unpolarized spectra on light coming exclusively from the magnetic fluxtubes. As (2.4) has been derived, it refers to the case that the magnetic element has been spatially resolved. In the real unresolved case V should be replaced by its average $\langle V\rangle$ over the resolution element. From (2.3) and (2.2) we see that $\langle V\rangle$ is obtained by performing the average $\langle B\partial I_V/\partial\lambda\rangle$. If we assume that $\partial I_V/\partial\lambda$ is independent of B whenever $B\neq0$ (i.e. $V\neq0$), the average to be formed becomes $\langle B\rangle\partial\langle I_V\rangle/\partial\lambda$. Thus we retrieve (2.4) if we replace B by $\langle B\rangle$ in $\Delta\lambda_H$ and I_V by $\langle I_V\rangle$. For a more realistic fluxtube, however, there will be correlated variations of the field strength B and the thermodynamic properties across the fluxtube. The calculated I_V profiles will therefore be a weighted average over the fluxtube cross section, with regions which have a stronger magnetic field giving a larger contribution. The I_V profiles are naturally also averaged over the time span of a measurement, over which period individual fluxtubes may have evolved.

It has been implicitly assumed in (2.4) that the total amount of magnetic flux does not vary with height. This makes $\Delta\lambda_H$ independent of height, and thus also of the wavelength in the line, allowing it to be moved outside the integration. This assumption can only be invalidated by the presence of very large canopies with diameters much larger than the resolution element, such as the ones proposed by Giovanelli (1980). Since practically all the lines considered in the present paper are formed below the temperature minimum, and thus below such canopies, we need not worry about their effects here.

As we have seen above, $\langle B\rangle$ in $\Delta\lambda_H$ acts as a scaling factor for the fluxtube line profiles derived through (2.4). The determination of $\langle B\rangle$ cannot, however, be carried out in an unambiguous and model independent manner using Fe I lines, since thermodynamic effects are strongly intermingled with area factor and magnetic field strength effects. Any depolarization due to the instrument will also falsify the results. We prefer not to bias the observations in advance and have therefore arbitrarily chosen a scale factor that corresponds to $\langle B\rangle=1$ G in (2.4). The derived line depths are accordingly incorrect by a factor equal to the actual value of $\langle B\rangle$ in G. As this correction factor is the same for all spectral lines, it will not affect our investigation of *differential* line profile effects when comparing different lines.

Of the innumerable spectral lines available, we have chosen for the present investigation the 402 Fe I lines selected by Stenflo and

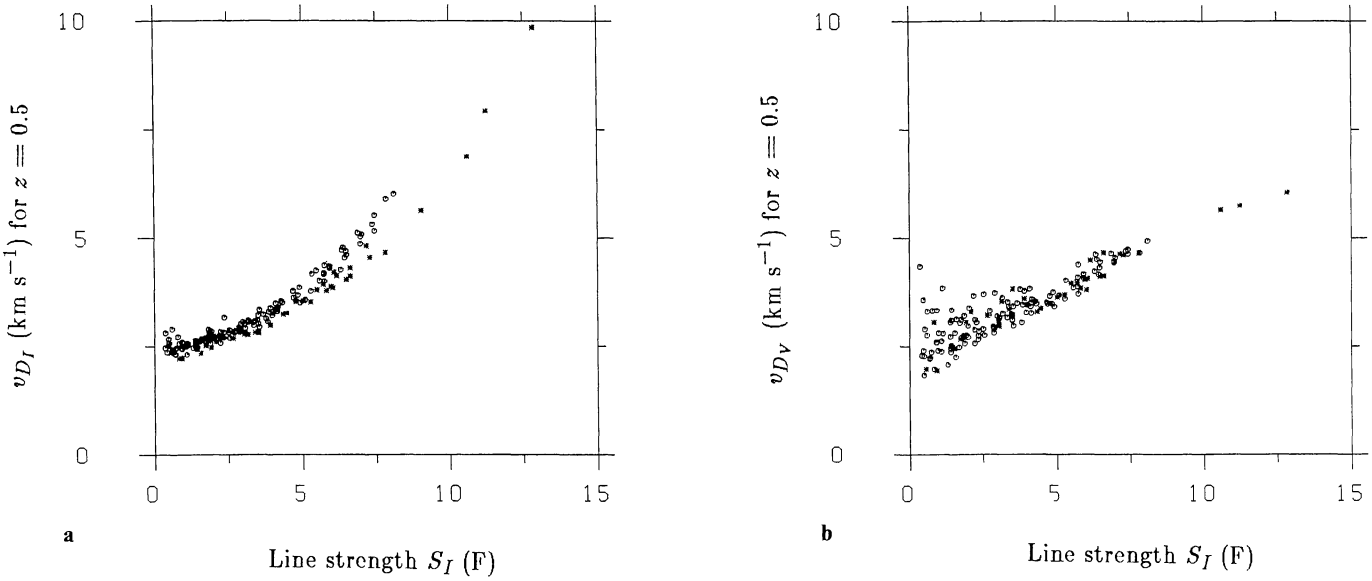

Fig. 2. Line width v_D (km s^{-1}) at the $z=0.5$ chord plotted as a function of I line strength S_I (Fraunhofer, F) for an enhanced network region. **a** v_{D_I}, width of Stokes I. **b** v_{D_V}, width of I_V (integrated V after the differential renormalization). Lines with $\chi_e<3$ eV are represented by a star, those with $\chi_e \geqq 3$ eV by a circle

Lindegren (1977) and have carried out the integration in (2.4) numerically for each of them.

Due to the observed difference in the areas of the blue and red wings of each Stokes V line profile (see Sect. 3 below), the level of the continuum on the blue and red sides of the integrated profile (I_V) is different (cf. Fig. 1). This, of course, makes no physical sense and only reflects the fact that (2.4) was derived for a static atmosphere, whereas the area asymmetry of a Stokes V profile, which causes this discrepancy in continuum level, requires the presence of a vertical velocity gradient inside the fluxtube (cf. Auer and Heasley, 1978). It is not possible to formulate an extended version of (2.4), including the effects of a general velocity field, without full prior knowledge of the velocity structure. In view of this fact we decided to resolve the discrepancy between the red and blue continua by averaging the two halves, weighing each half such that the continuum on both sides of the line appears at the same level [the geometrical mean of the two continua obtained via (2.4)]. Thus the values of Stokes V on the blue side of the zero-crossing wavelength λ_0 of the V profile have been multiplied by $\sqrt{A_r/A_b}$, the values of V on the red side of λ_0 by $\sqrt{A_b/A_r}$, before the integration in (2.4) has been carried out. A_r and A_b are the areas of the red and blue wings of the V profile, respectively.

The reason why we force the continua on both sides of the line to agree with each other is to be able to parameterize the so derived I_V profiles in the same way as we parameterize the unpolarized Stokes I spectrum (see Sect. 3 below). By parameterizing the Stokes V profiles via I_V we can treat the I and V spectra on an equal basis. In order to minimize the effects of artificially creating a single continuum level we have determined the parameters relating to the *velocity* structure directly from Stokes V and *not* from I_V.

2.3. Noise, blends, and Landé factors

Although the average noise level of the data is very low (close to 0.03%), it gets larger near the edge of the prefilter wavelength range and may in these regions affect the V profiles of the weaker lines. We have therefore eliminated all lines with maximum amplitudes of their V profiles less than 5σ of the noise level. This limit removes practically all the lines heavily influenced by noise although a few lines with V amplitudes greater than this limit had to be checked individually and removed due to their untypical behaviour in the scatter plots (which are presented in Sects. 3 and 4). Reasons for such untypical behaviour are blends or deviations from LS coupling.

Blends make themselves felt more strongly in our work than in the case of Stenflo and Lindegren (1977), because the V profiles are in general more sensitive to blends than the I profiles (Stenflo et al., 1984), and because the complete Stokes V profile has to be integrated, including the far wings. Very weak blends are not a big problem, since due to the approximate antisymmetry of the Stokes V profile, they only alter the profile in the region of the blend itself, i.e. usually out in the far wings, and thus do not affect our analysis. In some cases, however, the presence of blends has required the rejection of a particular line from our sample. Examples are: 5216.3 Å, 5022.2 Å, and 4637.5 Å.

Landé factors play a crucial role in the determination of the integrated V profile, I_V, as shown by (2.4) and (2.2). All lines with Landé factors of zero had to be omitted in the V analysis. An example is the 5434.53 Å line having an effective Landé factor of zero according to LS coupling. Landi Degl'Innocenti (1982) has found $g_{\rm eff}=-0.014$ using measured Landé factors for its upper and lower levels. Our data show no sign of this line in the V spectra, consistent with a $g_{\rm eff}$ of zero. It is the fourth strongest line in our sample, and a glance at Figs. 2a and b shows that it is present in the former figure (I line widths vs. I line strengths), but is missing in the latter (I_V line widths vs. I line strengths). The other lines with zero LS coupling Landé factors were also individually checked in the spectra. In each case the data were compatible with $g_{\rm eff}=0$, with the exception of the 4596.4 Å line, which will be discussed later.

An error in $g_{\rm eff}$ will cause I_V to be either too deep or too shallow, as I_V scales with the Landé factor. A scatter plot of I_V line depth, d_V, vs. I_V line strength, S_V, is therefore quite sensitive to departures from the correct value of $g_{\rm eff}$ caused by the breakdown of LS coupling. This may be the explanation why some lines lie many standard deviations from the mean in such scatter plots (for all the spectra containing these lines), although no blends are

Table 1. List of empirically determined Landé factors

Wavelength	Multiplet	$g_{\mathrm{eff}_{\mathrm{LS}}}$	$g_{\mathrm{eff}_{\mathrm{emp}}}$
4596.4113	823	0.00	0.9 ± 0.2
4918.0152	1070	0.50	0.9 ± 0.2
4945.6390	1113	0.33	0.7 ± 0.15
4995.4109	1113	−0.25	0.6 ± 0.15
5159.0637	1091	0.25	0.9 ± 0.2
5197.9385	1091	1.25	0.5 ± 0.1
5398.2860	1145	0.33	0.6 ± 0.1
5487.7512	1025	0.67	1.2 ± 0.2
5905.6759	1181	0.75	0.5 ± 0.1
5927.7919	1175	1.00	0.5 ± 0.1
6093.6457	1177	0.33	0.7 ± 0.15
6094.3766	1177	−0.25	0.6 ± 0.15

apparent, and the noise is insignificant. In Table 1 we list the lines for which we suspect the LS coupling Landé factors to be incorrect, together with our empirical estimates of the correct values. These estimates have been determined using the $\ln(d_V/d_I)$ vs. S_I (d_I and S_I are the line depth and strength of Stokes I) plots which will be discussed in detail in Sects. 3 and 4 (cf. Fig. 3). A Landé factor that is too small results in a value of $\ln(d_V/d_I)$ that is too large and vice versa, since d_V scales inversely with g_{eff} [according to (2.4)]. The correct value of the Landé factor is found by determining the line depth, d_V, that the line must have in order to lie on the average curve described by the rest of the points. If we denote the Landé factor as determined by LS coupling by $g_{\mathrm{eff}_{\mathrm{LS}}}$, the corresponding line depth of the I_V profile by $d_{V_{\mathrm{LS}}}$, the empirically determined Landé factor by $g_{\mathrm{eff}_{\mathrm{emp}}}$, and its corresponding I_V line depth by $d_{V_{\mathrm{emp}}}$, then the relation between $g_{\mathrm{eff}_{\mathrm{emp}}}$ and $g_{\mathrm{eff}_{\mathrm{LS}}}$ is of the form

$$g_{\mathrm{eff}_{\mathrm{emp}}}=g_{\mathrm{eff}_{\mathrm{LS}}}\exp\left(\ln\left(\frac{d_{V_{\mathrm{LS}}}}{d_I}\right)-\ln\left(\frac{d_{V_{\mathrm{emp}}}}{d_I}\right)\right). \tag{2.5}$$

It is possible that hidden blends may affect our results. The inherent scatter of the $\ln(d_V/d_I)$ vs. S_I plot also introduces some uncertainty. Our confidence in the g_{eff} values given in Table 1 is increased by the fact that in the cases when it has been possible to compare our results with those of other authors, we have found them to agree within the error limits. Landi Degl'Innocenti (1982) gives g_{eff} values for two of the lines in Table 1. For the 4945.6 Å line he finds $g_{\mathrm{eff}}=0.791$ as compared with our value of 0.7 ± 0.15. For the 4596.4 Å line, which has an LS coupling Landé factor of zero, his result is 0.753 whereas ours is 0.9 ± 0.2.

Stenflo et al. (1984) also looked at the Landé factors of a few lines. They used the 6093.6 Å line as a reference for determining the Landé factor of the 6094.4 Å line (LS coupling Landé factor $=-0.25$, which they showed to be obviously wrong, since its profile was only compatible with a positive value of g_{eff}), but found that the Landé factor of the 6093.6 Å line is itself not consistent with the g_{eff} of the 6096.7 Å line. They were unable to say which of these two lines had a correct g_{eff} value in LS coupling. Since our analysis does not rest on the comparison of individual lines, but rather on comparing single lines with the statistical mean of a large number of lines, we can resolve this dilemma. The 6096.7 Å line is found to have a Landé factor consistent with its LS coupling value, requiring the g_{eff} value of the 6093.6 Å line to be changed.

3. Statistical analysis

3.1. Parameterization of the line profiles

With the availability of a large number of spectral lines, the use of statistical methods to obtain information on fluxtube properties suggests itself. We follow Stenflo and Lindegren (1977) in choosing the following parameters to describe the I and I_V profiles (which have been normalized in units of the local continuum level): *(i)* the line depth, denoted by d_I and d_V, respectively. *(ii)* The lengths of four horizontal chords drawn at distances zd above line bottom [$v_{D_I}(z)$ and $v_{D_V}(z)$], with z having the values 0.1, 0.3, 0.5, and 0.7. These chord lengths are expressed in velocity units ($\mathrm{km\,s^{-1}}$, in terms of the Doppler width of a Gaussian profile having a chord length equal to the measured one). *(iii)* The line strength (S_I and S_V), given by the area of the line under the $z=0.5$ chord, expressed in Fraunhofer (area in wavelength units times $10^6/\lambda$).

The asymmetries of the Stokes V profiles require the introduction of further parameters. Thus we determine the amplitudes a and the areas A of both the blue and red Stokes V profile wings (a_b, a_r and A_b, A_r, respectively), and construct the absolute amplitude asymmetry, Δa, and the absolute area asymmetry, ΔA:

$$\begin{aligned}\Delta a&=a_b-a_r,\\ \Delta A&=A_b-A_r\end{aligned} \tag{3.1}$$

(a_b, a_r, A_b, and A_r are all positive). The relative asymmetries are obtained by simply dividing Δa or ΔA by the sum of the two amplitudes or areas, respectively: $(a_b-a_r)/(a_b+a_r)$ and $(A_b-A_r)/(A_b+A_r)$. It should be noted that these asymmetries refer to the original Stokes V profiles and *not* to I_V.

3.2. Scatter plots

Once the parameters have been determined, we can start looking for relations between them by plotting different combinations of them against each other. In order to accentuate the differences between the fluxtubes and their surroundings, differential methods are the most powerful. Thus we have studied the difference between the line widths of the I and I_V profiles [$v_{D_V}(z=0.5)-v_{D_I}(z=0.5)$] as well as the natural logarithm of their line depth ratios [$\ln(d_V/d_I)$] as functions of different parameters (cf. Sects. 4 and 5).

Let us, however, first show in Figs. 2a and b the line widths at the $z=0.5$ chord of the I and the I_V profiles, each vs. the line strengths, S_I, of the intensity profiles. The reason for not using S_V for the abscissa in Fig. 2b is the following: since the average field strength $\langle B\rangle$ is not a known quantity, the values of S_V cannot be directly compared with those of S_I, since the scales differ by a constant but unknown factor, as explained in Sect. 2. Using S_I as abscissa for both diagrams of Fig. 2 thus facilitates the comparison between the I and I_V data.

Several things are apparent in Fig. 2. First, after account has been taken of the greater scatter in the I_V line widths of weak lines, we notice that the I_V lines are narrower than their counterparts in the intensity spectrum. This is most striking for the strongest lines. Temperature effects, magnetic inhibition of convection (Gough and Taylor, 1966) leading to a lower microturbulence velocity inside the fluxtube, and magnetic broadening probably all play a role in producing this difference. Further analysis (cf. Sect. 4) shows, however, that the temperature effects dominate.

We also note that the splitting of the line width curve due to the excitation potentials χ_e of the lines (lines with $\chi_e<3$ eV are marked by a star, those with $\chi_e\geqq3$ eV by a circle in all the plots of the

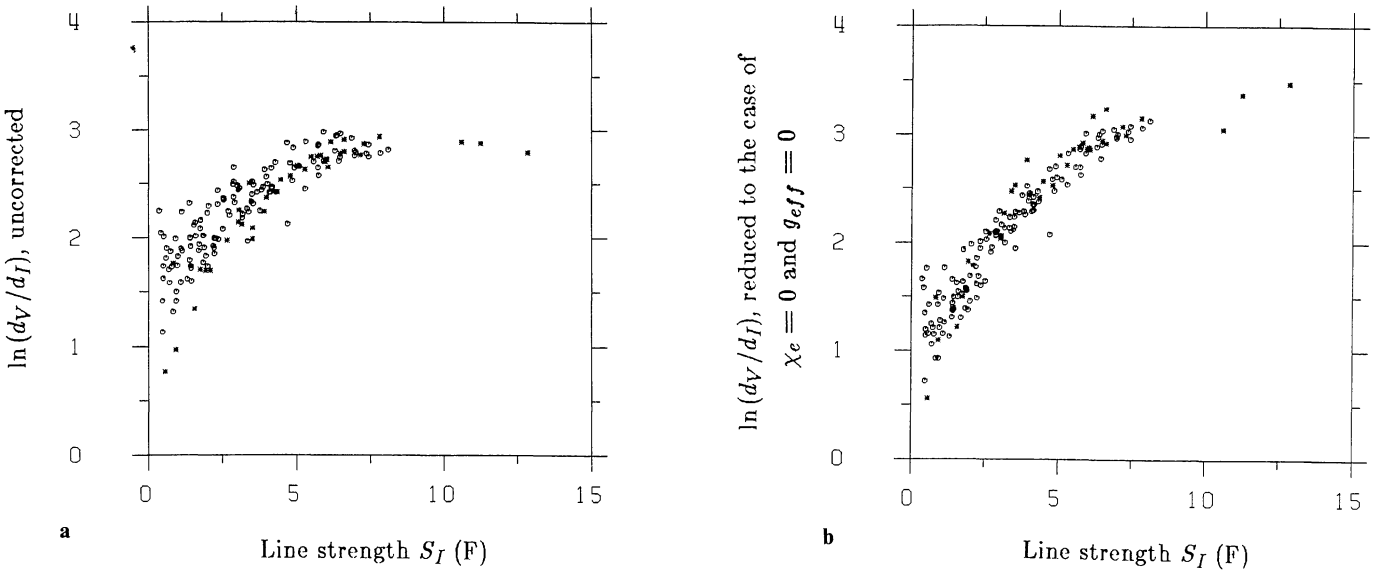

Fig. 3. $\ln(d_V/d_I)$ vs. S_I, where d_V and d_I are the line depths of the I_V and I profiles, respectively, and S_I is the line strength of the I profiles. **a** Raw data for an enhanced network region. **b** The same data after the application of (3.4) has reduced them to the case that $\chi_e=0$ and $g_{\rm eff}^2\lambda^2/v_0^1=0$

present paper) seen in Fig. 2a (cf. Stenflo and Lindegren, 1977) is absent in Fig. 2b. This phenomenon will be interpreted when discussing the V profile asymmetries.

The small scatter in Fig. 2a as compared with Fig. 3 of Stenflo and Lindegren (1977) illustrates the superiority of the FTS spectra over the Jungfraujoch atlas data that they used.

Stenflo and Lindegren (1977) showed that the dependence of v_{D_I} (unless stated otherwise v_{D_I} and v_{D_V} will from now on always represent the line widths at the $z=0.5$ chord) on line strength, excitation potential, and Landé factor may be expressed by a regression equation of the following form:

$$v_{D_I}=x_1+x_2S_I+x_3S_I^2+x_4v_0\chi_e+x_5g_{\rm eff}^2\lambda^2/v_0\,. \tag{3.2}$$

The x_i are the regression coefficients and v_0 is a second order polynomial fit of v_D to S. We have omitted their sixth term, $\langle g_{\rm eff}^2\rangle\lambda^2/v_0$, which essentially takes into account the dependence of line width on wavelength. This is permissible in our case, since we are not looking for such minute effects as the line broadening due to a weak, tangled magnetic field. We have verified numerically that this term has no significant effect on the other coefficients.

The same regression formula describes the dependence of v_{D_V} and $v_{D_V}-v_{D_I}$ on S_I, χ_e, and $g_{\rm eff}$ very well, too. Its use confirms our suspicion from Fig. 2b that v_{D_V} is practically independent of χ_e. It also shows a significant dependence of both v_{D_V} and $v_{D_V}-v_{D_I}$ on $g_{\rm eff}^2\lambda^2/v_0$ consistent with the presence of kG fields inside the fluxtubes. The interpretation of x_5 in terms of magnetic field strengths is, however, somewhat different from Stenflo and Lindegren (1977), who considered a turbulent magnetic field.

For the further analysis and to enable a crude interpretation of our data, it is convenient to introduce a two component model. Thus the photosphere is assumed to consist of a magnetic component, covering a fraction α of the surface and a non-magnetic component covering the remaining fraction $(1-\alpha)$. We will call α the area factor or filling factor. It is assumed that within the magnetic component the field strength, B, is constant, and in the non-magnetic component $B=0$. The model atmospheres that will be used for the two components are described below in Sect. 4.1. Empirical evidence for the validity of a two-component approach can be found in e.g. Stenflo (1976) and Stenflo and Harvey (1984), where the observed small statistical spread in the intrinsic fluxtube field strengths and line weakenings is demonstrated.

To derive a simple analytical relation between field strength B in the fluxtube and the coefficient x_5 in the $v_{D_V}-v_{D_I}$ regression equation, we use our two-component model for the longitudinal magnetic field, assume the line profile to be Gaussian and the Zeeman splitting to be much smaller than the line width. We furthermore assume that in the case of zero Landé factor, the line depth in the magnetic regions is δ times the line depth outside the fluxtubes ($\delta<1$ in the case of line weakening), but that the line width is unchanged (this last assumption is fulfilled by all but the strongest lines, as Fig. 8 shows). With these assumptions, using the Taylor expansion (2.1) and the definition (2.4) of I_V, we find

$$B=\frac{(3x_5)^{1/2}}{kc}(1-3\delta\alpha)^{-1/2}\,, \tag{3.3}$$

where $k=4.67\,\mathrm{km^{-1}\,G^{-1}}$, and c is the speed of light. The factors 3 in (3.3) appear because the magnetic broadening of I_V and I is due to the second terms in their respective Taylor expansions and the numerical coefficients of the two relevant terms differ by a factor of 3.

For $\ln(d_V/d_I)$ the regression equation giving the best results is the following:

$$\ln(d_V/d_I)=x_1+x_2S_I+x_3S_I^2+x_4\chi_e+x_5S_I\chi_e+x_6g_{\rm eff}^2\lambda^2/v_0^2\,. \tag{3.4}$$

Fig. 3a shows $\ln(d_V/d_I)$ plotted against S_I for an enhanced network region. It can be seen that the scatter increases considerably with decreasing line strength. However, a considerable portion of this is not random noise, but is of solar origin, as Fig. 3b shows. In this diagram we have again plotted $\ln(d_V/d_I)$ vs. S_I, but with the dependence of the points on excitation potential and Landé factor removed using (3.4). The main contribution to the scatter of the points in Fig. 3a comes from their dependence on excitation potential. Both the 4th and 5th terms are needed to correctly reproduce this χ_e dependence.

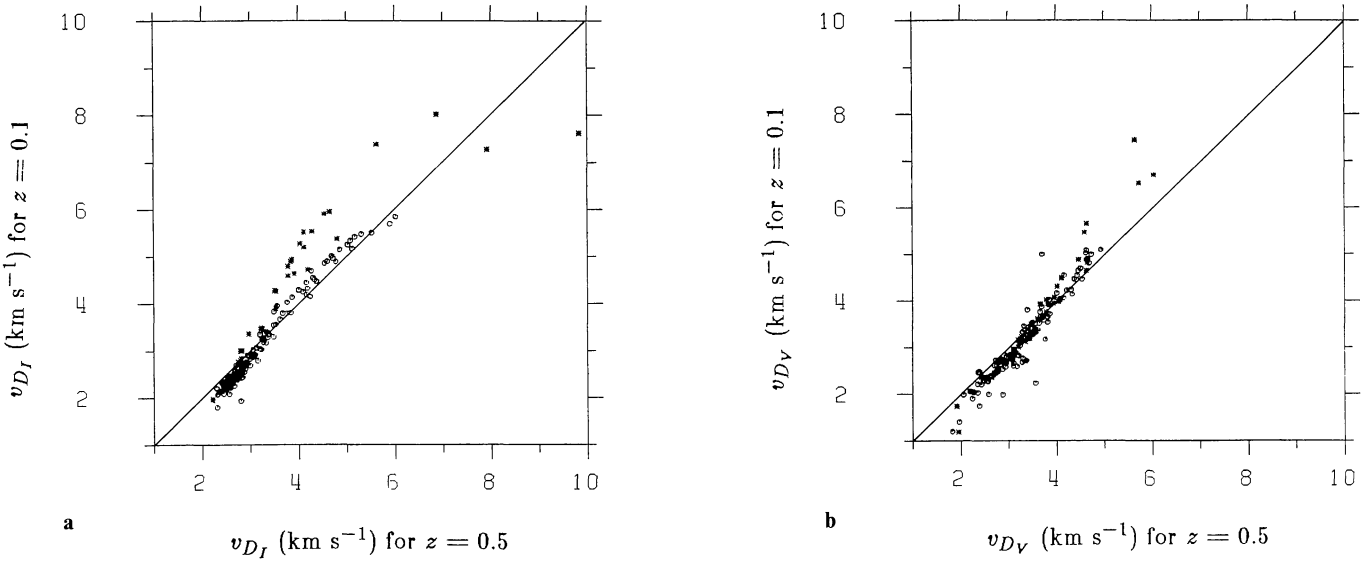

Fig. 4. Line widths at the $z=0.1$ chord plotted vs. line widths at the $z=0.5$ chords for an enhanced network region. **a** I profiles. **b** I_V profiles

The interpretation of the x_6 term in (3.4) is very similar to that of the x_5 term in (3.2). Notice, however, that the dependence of this term on line width goes with $1/v_0^2$ as compared with the $1/v_0$ dependence of the x_5 term of (3.2). Making the same assumptions as were made for the derivation of (3.3) the following dependence of $\ln(d_V/d_I)$ on the magnetic field is found:

$$\ln(d_V/d_I)=\ln I_c+\ln\delta+\alpha(1-\delta)-\frac{1}{3}\frac{v_H^2}{v_D^2}(1-3\delta\alpha), \tag{3.5}$$

where α and δ have the same meaning as in (3.3), I_c is the unknown level of the continuum of the I_V spectrum, v_D is the line width, and v_H is the Zeeman broadening expressed in velocity units. The first three terms on the right side of (3.5) are independent of the magnetic field and of line parameters if the lines chosen are of approximately the same strength and excitation potential. Thus only the last term is of consequence for the determination of the magnetic field strength. For the choice of regression terms used in (3.4) it gives a relation between the magnetic field and regression coefficient x_6 identical to that of (3.3) if we replace x_5 by x_6:

$$B=\frac{(3x_6)^{1/2}}{kc}(1-3\delta\alpha)^{-1/2}. \tag{3.6}$$

In Fig. 4a and b the line width at the $z=0.1$ chord has been plotted vs. the line width at the $z=0.5$ chord, for the I and I_V profiles of a network element. These diagrams provide information on the shape of the line profile. By virtue of the definition of v_D, a line with a Gaussian profile would fall on the 45° line in the diagram. Lines with more U-shaped profiles lie above this line, whereas lines with more V-shaped profiles lie below it.

The main difference between the behaviour of the I and I_V profiles appears to be that the I_V profiles do not show any significant distinction between lines of different excitation potentials, in contrast to the I profiles. The different behaviour of $\chi_e<3$ eV and $\chi_e\geqq 3$ eV lines in Fig. 4a is a non-LTE effect. The $\chi_e<3$ eV levels, being metastable, are overpopulated as compared with the higher levels (Lites, 1972). An increase in temperature inside the fluxtube might explain the merging of the $\chi_e\geqq 3$ eV and $\chi_e<3$ eV curves of the I_V diagram, since it would raise the population of the higher levels relative to the lower ones.

Let us now consider the amplitude asymmetry of the Stokes V profiles. Figure 5a shows the absolute amplitude asymmetry, Δa, for a plage plotted vs. the I line strength, S_I. Basically, this diagram tells us something about the height variation of the velocity gradient inside the fluxtube. If we assume the magnetic field to be vertical, then the field strength must vary with height as well (Auer and Heasley, 1978). The large scatter of the points can again be reduced significantly by using the regression expression

$$\Delta a=x_1+x_2S_I+x_3S_I^2+x_4S_I^3+x_5S_I\chi_e, \tag{3.7}$$

to subtract the dependence on excitation potential. The result is shown in Fig. 5b. This dependence of the asymmetry on excitation potential is not very surprising, since the heights of formation of lines with higher excitation potentials can be substantially different from those of lines with lower χ_e having the same line strength. They can thus be formed in regions with different velocity field gradients, and can therefore show different amplitude asymmetries.

This strong dependence of the amplitude asymmetry on excitation potential suggests an explanation of the difference in behavior of v_{D_I} and v_{D_V} with respect to χ_e that was illustrated in Fig. 2. A velocity gradient will not only break the anti-symmetry of the Stokes V profiles, but will also broaden the lines. If we make the reasonable assumption of approximate proportionality between the amplitude asymmetry and the increase in line width induced by the velocity gradient, then a look at Fig. 5a tells us that the profiles of lines of low excitation potential should be more broadened than those of high excitation potential, which is just the effect needed to explain Fig. 2b. The straightness of the curve in Fig. 2b also suggests this explanation. The points of the intermediately strong lines seem to have been shifted upwards, changing the shape of the curve from a parabola into an approximately straight line. Since the same intermediately strong lines are the most asymmetric ones, they should also be the most broadened ones.

Let us finally look at the relative V asymmetries (in the original Stokes V, *not* in I_V). Figure 6a and b show the relative area and amplitude asymmetries for a plage, plotted as functions of S_I. The solid curves drawn through the data points are smoothed averages (cubic spline fits). We notice the different shapes of the two curves.

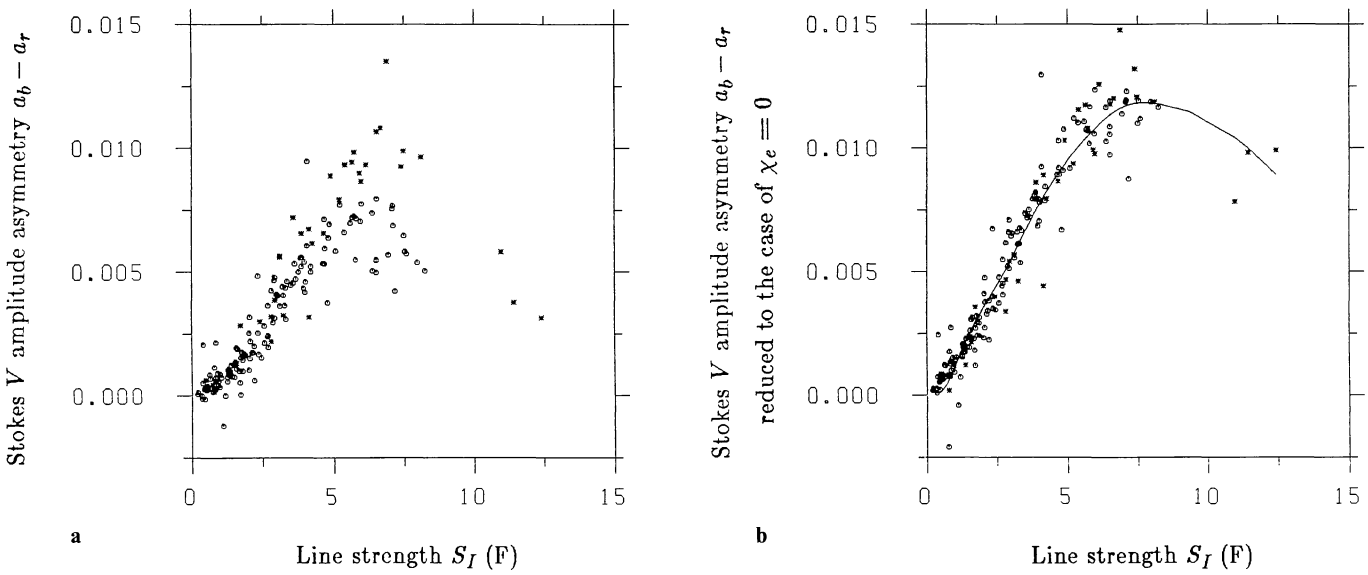

Fig. 5. Absolute amplitude asymmetry $\Delta a = a_b - a_r$, plotted vs. I line strength, S_I. a_b and a_r are the amplitudes of the blue and red wings of V. **a** Raw data for a plage region. **b** The same data reduced to the case that $\chi_e = 0$ using the regression (3.7). The smoothed average (cubic spline) is drawn as well

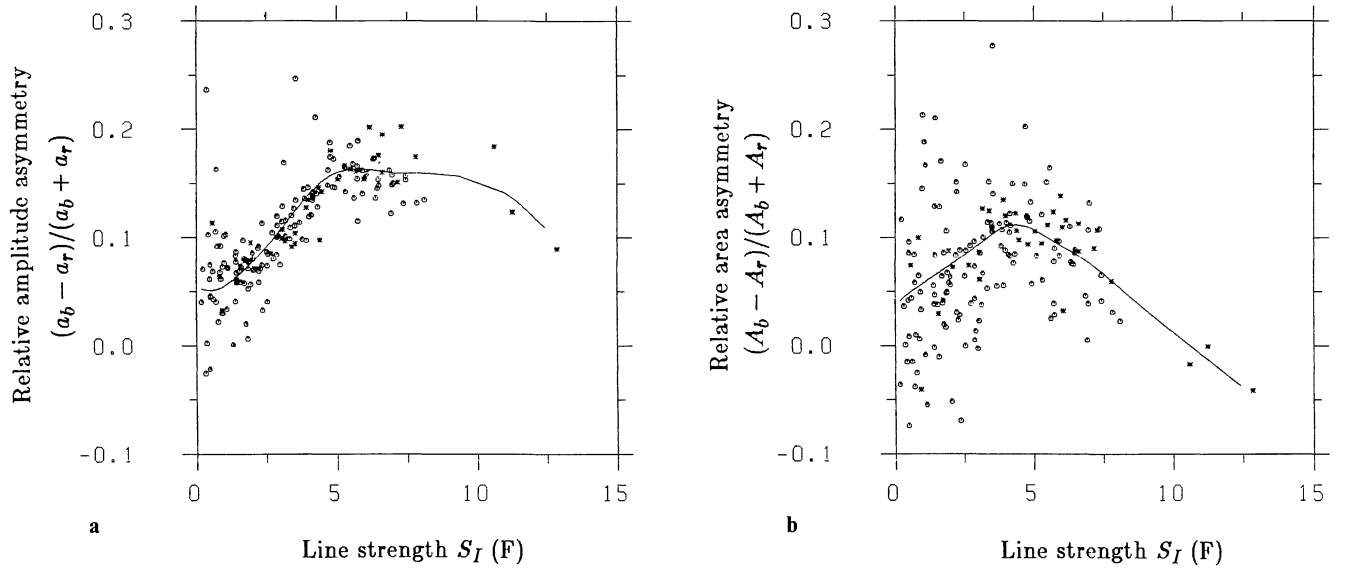

Fig. 6. a Relative amplitude asymmetry, $(a_b - a_r)/(a_b + a_r)$, vs. S_I for a plage. **b** Relative area asymmetry, $(A_b - A_r)/(A_b + A_r)$, vs. S_I for the same plage as in **a**. The solid curves are smoothed averages (cubic splines)

The relative area asymmetry actually becomes negative for the strongest lines of our sample, while the relative amplitude asymmetry remains positive. The reproduction of these curves should present a major challenge to any model of the velocity field inside a fluxtube.

4. Diagnostic contents of the scatter plots

In order to unleash the full power of our statistical approach as a diagnostic tool of fluxtube properties we have to make use of model calculations. Only by comparing curves produced by a set of models with the scatter plots can we extract more quantitative information.

4.1. Fluxtube model

Before making any radiative transfer calculations we have to specify the atmosphere to be used, i.e., we have to build a fluxtube model. For exploratory purposes, to provide a concrete understanding of the diagnostic contents of the scatter plots, we have, in the present paper, used a very simple, static, one dimensional model containing four free parameters. As the reference atmosphere we have chosen the HSRASP, which is a downwards extension of the HSRA (Gingerich et al., 1971) obtained by matching the HSRA to Spruit's (1974) convection zone model (cf. Chapman, 1979). The fluxtube atmosphere is first established in the absence of a magnetic field, i.e., with a Wilson depression $Z_W = 0$. The parameters determining the temperature

structure are $\Delta T_{\rm top} = T_{\rm fluxtube} - T_{\rm HSRA}$ at $\tau_{5000}({\rm HSRA}) = 10^{-4}$ and $\Delta T_{\rm bot} = \Delta T$ at $\tau_{5000}({\rm HSRA}) = 1$. The temperature difference, ΔT, as a function of height, Z_0, is found by linear interpolation between $\Delta T_{\rm top}$ and $\Delta T_{\rm bot}$. The temperature inside the fluxtube is thus $T_{\rm fluxtube}(Z_0) = T_{\rm HSRA}(Z_0) + \Delta T(Z_0)$. The pressure inside the tube is simply the outside pressure, and the density is calculated using the equation of state of an ideal gas. The whole atmosphere is then shifted downwards by Z_W, which we regard as the Wilson depression (here defined as the height difference between levels with the same pressure inside and outside the fluxtube): $Z = Z_0 - Z_W$. It should be noted that in this model the Wilson depression is in general not the difference in heights between the levels with $\tau_{5000} = 1$ inside and outside the fluxtube. The magnetic field is determined from the resulting pressure difference:

$$B = \sqrt{8\pi(P_{\rm HSRA} - P_{\rm fluxtube})}\,. \tag{4.1}$$

Once we have fixed Z_W, $\Delta T_{\rm top}$, $\Delta T_{\rm bot}$, and $f = \xi_{t_{\rm fluxtube}}/\xi_{t_{\rm HSRA}}$ (the ratio of the microturbulence velocities inside and outside the fluxtube), the model atmosphere is uniquely determined. The electron pressure and the opacity can be extracted from tables and graphs in Baschek and Scholz (1982), Allen (1973), and Unsöld (1968).

4.2. *Radiative transfer*

The radiative transfer code used to calculate the I and V profiles has been described by Beckers (1969a, b). It is an LTE code capable of calculating all 4 Stokes profiles for any model atmosphere and for any magnetic and velocity field variations along the line of sight. We have calculated the profiles for a series of 96 hypothetical Fe I lines at a wavelength of 5000 Å, having different oscillator strengths, excitation potentials, and Landé factors.

First, we calculated the line profiles using the HSRASP as our model atmosphere. This was done primarily to find a suitable function for $\xi_t(Z)$, since the widths of the calculated lines depend strongly on this parameter and very little reliable data are available for its height variation. In order to reproduce Fig. 2a faithfully we had to increase ξ_t in the upper part of the photosphere. This is in contrast to the results presented in the review by Gurtovenko (1975), which show a monotonic decrease of the microturbulence velocities with height, at least up to $\log\tau_{5000} = -2.5$. Our increase of ξ_t near the temperature minimum may be a result of non-LTE effects, although Holweger (1973) points out that non-LTE effects should not falsify the value of the microturbulence velocity. Fortunately, the absolute value of $\xi_t(Z)$ is not so important, since those of our results which depend on line widths have all been derived from $v_{D_V} - v_{D_I}$ plots, where only the difference between the microturbulence velocities inside and outside the fluxtube play a role.

The profiles of the 96 hypothetical Fe I lines were then calculated for 27 different fluxtube models. Finally, the line parameters described in Sect. 3.1 were determined for the theoretical lines as well.

4.3. *Comparison of theory and observations*

The comparison of sets of lines calculated using different fluxtube models with observed data gives us an idea of the diagnostic contents of the different scatter plots. The two main groups of scatter plots that have been compared with the calculations are the ones in which either $v_{D_V} - v_{D_I}$ or $\ln(d_V/d_I)$ are plotted against one of the parameters: χ_e, S_I, or $g_{\rm eff}^2\lambda^2/v_0$ [$g_{\rm eff}^2\lambda^2/v_0^2$ in the case of $\ln(d_V/d_I)$]. In most of the cases we have used the regression expressions (3.2) and (3.4) to reduce the influence of the passive parameters on a given plot. Thus, for example, in the plots having χ_e as abscissa the data have been reduced to values corresponding to lines with $S_I = 0$ and $g_{\rm eff} = 0$. In the following we will give a general discussion on the diagnostic contents of the different plots, leaving the discussion of individual models and of the derived properties of plages and the network to Sect. 5.

4.3.1. $\ln(d_V/d_I)$ vs. S_I

This relation was plotted in Fig. 3 (Sect. 3). The average value of $\ln(d_V/d_I)$ gives a measure of the net magnetic flux through the observed region (spatial resolution element). A change in flux or average field strength $\langle B\rangle$ shifts all the points up or down.

The *shape* of the plot is, however, not affected by either the field strength or the area factor. It provides information on the temperature structure. Since the relative line depth scales of the V and I profiles depend on the value of $\langle B\rangle$, which is not known (see Sect. 2), the temperature information in this plot is contained in the gradient of the plotted curve and not in its absolute values. The decrease of $\ln(d_V/d_I)$ with decreasing line strength (S_I in Fig. 3) is a result of the line depths of the weak lines being much more dependent on temperature than those of the strong lines. A temperature increase inside the fluxtube just below the temperature minimum (leaving the temperature lower down unchanged) shifts the points representing the stronger lines downwards, leaving the weaker lines unchanged. This makes the whole plot flatter. A temperature increase in the lower region of the atmosphere shifts the weaker lines downwards, making the plot steeper. Since the points approach an asymptotic level with increasing line strength, the plot is considerably more sensitive to temperature changes in the lower part of the atmosphere than higher up. If we, for example, increase the temperature in our linear $\Delta T(Z_0)$ model at the top from $\Delta T_{\rm top} = +100$ K to $\Delta T_{\rm top} = +300$ K, we obtain a steeper curve, which is the opposite to what one would naively expect. This is due to the fact that the effect of this temperature increase on the depths of the strong lines formed higher up is much smaller than the effects of the smaller temperature increase induced by it (through linear interpolation) lower down in the atmosphere on the depths of the weak lines formed there. The circumstance that calculations based on our static model fit this plot relatively well indicates that it is only weakly dependent on the velocity structure in the fluxtube.

4.3.2. $\ln(d_V/d_I)$ vs. χ_e

This plot also contains information on the temperature structure. For a fixed temperature at $\tau_{5000} = 10^{-4}$ an increase in temperature at $\tau_{5000} = 1$ makes the relation steeper. A temperature increase at $\tau_{5000} = 10^{-4}$ produces this effect to an even greater extent. A change of 400 K at the top of the photosphere has the same effect as a change of 700 K at the bottom. As is the case for the $\ln(d_V/d_I)$ vs. S_I plot, only the slope of the relation is temperature dependent. Figure 7 shows $\ln(d_V/d_I)$ vs. χ_e for four data sets and for 5 fluxtube models. The increase in gradient caused by increasing $\Delta T_{\rm bot}$ is clearly visible.

4.3.3. $v_{D_V} - v_{D_I}$ vs. S_I

This plot, illustrated in Fig. 8, has not been reduced to $\chi_e = 0$ for reasons stated below. The points are sensitive to the temperature structure, the microturbulence velocity and the macroscopic velocity field. Unfortunately, the effects caused by temperature and

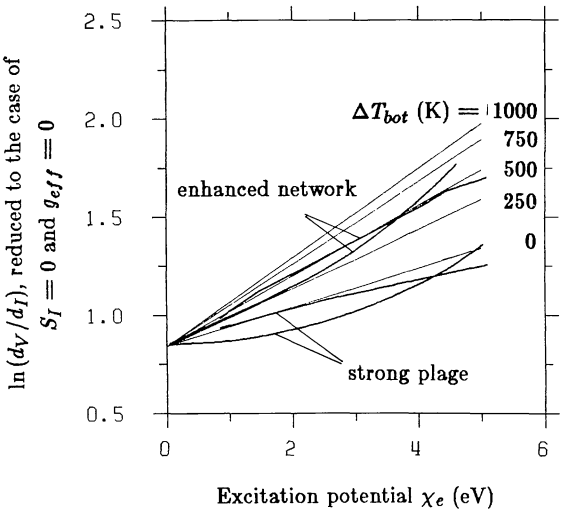

Fig. 7. The four thick lines represent the average (cubic spline fit) of $\ln(d_V/d_I)$ vs. χ_e when the data have been reduced to the case that $S_I=0$ and $g_{\rm eff}=0$. The two curves with the steeper slope correspond to enhanced network regions, the other two correspond to plages. The thin lines are theoretical curves calculated from models with $\Delta T_{\rm top}=500$ K and $\Delta T_{\rm bot}=0$, 250, 500, 750, and 1000 K, in the order of increasing slope, for lines with $g_{\rm eff}=0$ and $S_I\approx 0$. The curves have been arbitrarily normalized such that they coincide at $\chi_e=0$

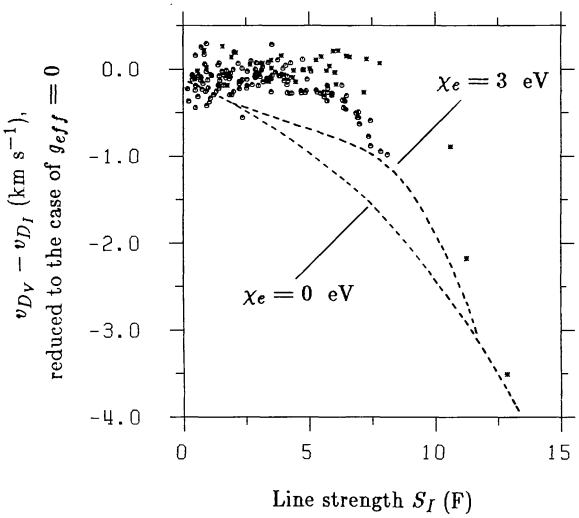

Fig. 8. $v_{D_V}-v_{D_I}$ at the $z=0.5$ chord vs. S_I for a plage. The data points have been reduced to the case that $g_{\rm eff}=0$ (but not to $\chi_e=0$). The dashed lines are curves calculated from a model with $\Delta T_{\rm top}=500$ K and $\Delta T_{\rm bot}=250$ K, Wilson depression $Z_W=50$ km, and $f=\xi_{f_{\rm fluxtube}}/\xi_{f_{\rm photosphere}}=0.7$ [best model for fitting the $\ln(d_V/d_I)$ vs. S_I plot for this plage]. Both theoretical curves are for lines with $g_{\rm eff}=0$. The lower theoretical curve has been calculated for lines with $\chi_e=0$ eV, the upper curve for lines with $\chi_e=3$ eV

velocity structures are entangled, making it difficult to gain temperature information without first having a reliable model for the velocity field. This means that our model calculations, which have been carried out for a static atmosphere, have no hope of reproducing the observations. The weakest and the strongest lines are fitted reasonably well by the same models which also give good fits to the line depth data, but the results for intermediately strong lines deviate rather strongly from the data. This is precisely the effect predicted in Sect. 3 when discussing the plots of the V height asymmetry. The different dependences of v_{D_V} and v_{D_I} on χ_e apparent in Fig. 2 appear in this plot, too, causing lines of higher χ_e to lie below those of lower χ_e. The calculations, on the other hand, result in exactly the opposite χ_e dependence for *all* our models, strongly supporting the suggestion that this effect is a result of the coupling of the temperature structure with a velocity field gradient (cf. the discussion of Fig. 5). It certainly cannot be explained by a temperature change alone.

The plot is more sensitive to temperature changes at the top than at the bottom of the photosphere, since the widths of the weak lines are relatively insensitive to temperature changes, as our model calculations indicate. All models give a good fit to the weak lines, which means that only the strong lines give any temperature information. A change in T of 800 K at the $\tau_{5000}=1$ level would, in our linear $\Delta T(Z_0)$ models, result in the same change in line widths of the strongest lines that a change of about 200–300 K at the top of the photosphere would cause. The diagram becomes practically insensitive to temperature for large values of $\Delta T_{\rm top}$, since then even the strongest lines in our sample are so weakened that they lie in the weak line regime.

The microturbulence velocity also affects the diagram. In contrast to the temperature the microturbulence velocity also changes the widths of the weak lines, allowing us in principle to make a very rough estimate of f (ratio of the microturbulence velocities inside and outside the fluxtube) at the lower levels of the atmosphere. However, the large scatter of the points and the unknown amount of broadening due to macroscopic velocity fields make this estimate very uncertain.

4.3.4. $v_{D_V}-v_{D_I}$ vs. χ_e

This plot verifies the linear trend caused by the coupled temperature-velocity structure that was predicted in the discussion of the $v_{D_V}-v_{D_I}$ vs. S_I diagram in Sect. 4.3.3.

4.3.5. $\ln(d_V/d_I)$ vs. $g_{\rm eff}^2\lambda^2/v_0^2$

The main information content of this plot, after the line strength dependence has been subtracted, is the magnetic field strength near the $\tau_{5000}=1$ level, which can be determined either using (3.6) or through comparison with model calculations. The decrease in depth of the I_V lines with increasing $g_{\rm eff}^2\lambda^2/v_0^2$, as seen in Fig. 9a for a plage, is due to Zeeman saturation. The theoretical curves have a weak dependence on the assumed temperature structure. For example a change in temperature by 500 K at the $\tau_{5000}=1$ level changes the magnetic field strength by about 100 G. A comparable change at the temperature minimum region has an even smaller effect, since the data points have all been reduced to the case of zero line strength. A systematic difference in the field strengths derived using (3.6) and those obtained through comparison of the theoretical curves with the data appears to exist and will be discussed in Sect. 5.2.

4.3.6. $v_{D_V}-v_{D_I}$ vs. $g_{\rm eff}^2\lambda^2/v_0$

This plot (Fig. 9b) determines the Wilson depression or, equivalently, B near $\tau_{5000}=1$. The Zeeman broadening can thus be used directly to determine a field strength in the kG range using (3.3). The magnetic field can also be determined using model calculations (cf. Fig. 9b). In this case a weak dependence on the

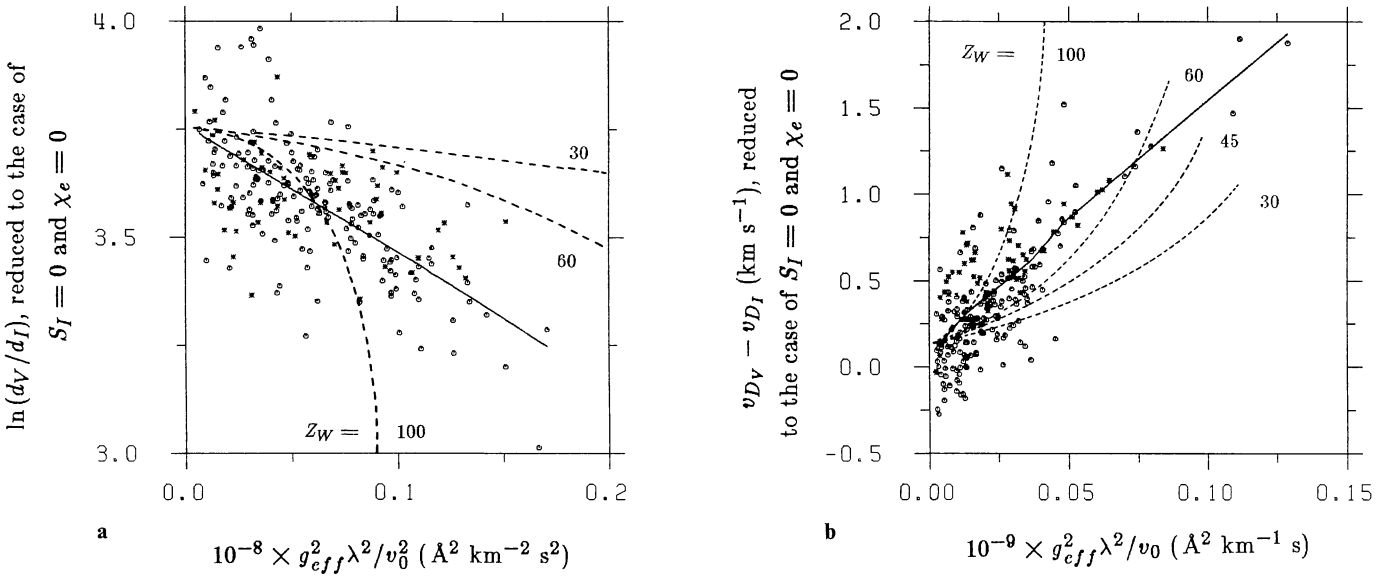

Fig. 9. a $\ln(d_V/d_I)$ vs. $g_{\rm eff}^2\lambda^2/v_0^2$, reduced to the case that $S_I=0$ and $\chi_e=0$ for a plage. The solid line is the average (cubic splines fit) of the data. The dashed curves have been calculated using models with $\Delta T_{\rm top}=500$ K, $\Delta T_{\rm bot}=250$ K, $f=0.7$, and Wilson depression $Z_W=30$, 60, and 100 km. **b** $v_{D_V}-v_{D_I}$ vs. $g_{\rm eff}^2\lambda^2/v_0$, reduced to the case that $S_I=0$ and $\chi_e=0$ for the same plage as in **a**. The solid line is again the smoothed average. The dashed curves represent calculations using models with $Z_W=30$, 45, 60, and 100 km

temperature structure occurs, of about the same magnitude as in the $\ln(d_V/d_I)$ vs. $g_{\rm eff}^2\lambda^2/v_0^2$ diagram. A change of ξ_t does not affect the determination of Z_W, since it just shifts the plot up or down without changing its slope. The magnetic field values determined from this plot are consistent with those obtained from the $\ln(d_V/d_I)$ vs. $g_{\rm eff}^2\lambda^2/v_0^2$ diagram (Fig. 9a). Again the value of B depends on the method used. This discrepancy will also be discussed in Sect. 5.2.

It is interesting to note that if we do not reduce this plot to $S_I=0$, then it is in principle possible to determine the height structure of the magnetic field, given a sufficient number of lines with different Landé factors and different line strengths. Unfortunately, our sample does not contain a sufficient number of strong lines with large $g_{\rm eff}$ to allow this plan to be carried out.

5. Comparison of plage and network properties

Using the diagrams discussed in the last section, we can now try to set some constraints on the properties of plages and network regions. Emphasis will be placed on direct comparison of the observations of the different regions, to demonstrate their similarities and differences.

5.1. *Thermal properties*

Line weakening measurements have indicated an increase in temperature inside the magnetic elements throughout most of the photosphere. The exact value of this temperature enhancement seems, however, to depend strongly on the technique used to determine it. For example Chapman (1977, 1979) finds that the plage temperature excess is around 1000 K at $\tau_{5000}=10^{-4}$, whereas Shine and Linsky (1974) find an excess of only 200 K at that level and none at $\tau_{5000}=1$. Stenflo (1975), on the other hand, arrives at a temperature excess of 800 K at $\tau_{5000}=10^{-4}$ and 100 K at $\tau_{5000}=1$ for both the network and plages. Koutchmy and Stellmacher (1977), studying network regions, derive a temperature enhancement of more than 2000 K at $\tau_{5000}=10^{-4}$ and still exceeding 1000 K at $\tau_{5000}=1$. Finally, Cook et al. (1983), using measurements in the 1700 Å region made with the HRTS rocket experiment find an intensity enhancement corresponding to a temperature excess of 300–400 K in both the network (bright points) and plage regions, with the filling factors of the bright elements being larger in the plage. The limited spatial resolution (1.8 arc s) probably means that this value is a lower limit, but the expansion of the fluxtubes with height may make them better spatially resolved at the height at which the 1700 Å spectrum is formed.

Our analysis shows that models with a temperature excess of 500 K at the $\tau_{5000}=10^{-4}$ level can reproduce the data reasonably well, considering the simplicity of the models. Fig. 10 shows the smoothed mean curves of $\ln(d_V/d_I)$ vs. S_I for our four different regions on the sun, normalized such that all curves coincide for the strongest lines. The curves representing fluxtubes in plages are much flatter than those of network elements, indicating that the plages have lower temperatures, at least over part of the photospheric height range. Also plotted in Fig. 10 are five theoretical curves produced from models with $\Delta T_{\rm top}=500$ K and $\Delta T_{\rm bot}=0$, 250, 500, 750, and 1000 K, respectively. These values correspond to temperatures 0, 100, 200, 300, and 400 K in excess of the quiet sun temperature at their respective $\tau_{5000}=1$ levels, since a temperature enhancement leads to a shift of the height of the $\tau_{5000}=1$ level. For the assumed value of $\Delta T_{\rm top}$ a network element seems to be about 400–800 K hotter than a plage fluxtube at the depth of one Wilson depression below $\tau_{5000}=1$ in the quiet photosphere, i.e. about 50 km. This result is in contrast to the models proposed by Stenflo (1975) and by Stellmacher and Wiehr (1979), which assume the same temperature and magnetic structures for plages and network regions.

To support and confirm these results we will compare the above models with other temperature sensitive diagrams. In Fig. 7 the smoothed mean of the $\ln(d_V/d_I)$ values have been plotted vs. excitation potential. Again the network gives a steeper curve, a

trend that is duplicated by the model curves having higher temperatures at the bottom of the photosphere. The agreement between the model predictions and the observations is, however, not perfect. The models tend to give too steep a slope. The reason for this inconsistency might lie in the large scatter of the data points underlying the smoothed curves of this diagram, but it could also be due to different thermal properties than our crude models assume. If we keep $\Delta T_{\rm top}=500$ K, then $\Delta T_{\rm bot}$ should be lower than suggested by the diagram of $\ln(d_V/d_I)$ vs. S_I. However, our assumption for the temperature at $\tau_{5000}=10^{-4}$ may be wrong. In this case a lower value of $\Delta T_{\rm top}$ might be the remedy.

A change in $\Delta T_{\rm top}$ may not be too large, however, since it would cause the model to come into conflict with either the $v_{D_V}-v_{D_I}$ vs. S_I diagram of Fig. 8 for too small temperature excesses, or with the $\ln(d_V/d_I)$ vs. χ_e diagram for too high temperatures. Thus the differences between plage and network can only be reproduced if the fluxtubes in plages are cooler than those in the network, at a depth of one Wilson depression below $\tau_{5000}=1$ of the photosphere, by about 600 K. A difference of 400–500 K still exists after magnetic filling factor effects have been taken into account. The larger factor in plages means that the I profiles there show larger contributions from the fluxtubes. This makes the $\ln(d_V/d_I)$ curve flatter, simulating a slightly lower temperature at greater depths.

A comparison between the temperatures inside and outside the fluxtube at equal geometric heights $\Delta T(Z)$ (i.e., after taking into account the Wilson depression) suggests that $\Delta T(Z_0)$ should depart from linearity, since the linearity assumption would lead to large variations of $\Delta T(Z)$ in the lower regions, and we would expect the temperature of the fluxtube to approach the surrounding temperature at greater depths. The models fitting the network do indeed suggest such an approach of the temperature inside the tube to the outside value at the same geometrical depth. In the plages this effect is not yet visible at the maximum depth at which our models are still valid. This difference between network and plage fluxtubes is consistent with the idea that fluxtubes in plages are on the average larger than in the network. The higher number density of magnetic elements in plages may cause smaller tubes to coalesce, thus increasing their average diameters. Due to limited spatial resolution our spectra have contributions from many different fluxtubes simultaneously, and therefore, the average properties of these tubes are observed.

Simon and Zirker (1974) and Koutchmy and Stellmacher (1978) have shown that on a small scale the emission enhancements are not always cospatial with the magnetic field concentrations. With our two-component approach we obtain the *average* properties of the magnetic and non-magnetic components, and the $\Delta T(Z)$ that we find refers to the difference between these two components regardless of the morphology of the magnetic and brightness patterns. If these patterns are not entirely cospatial, our derived values of ΔT will underestimate the actual temperature difference between the fluxtubes and the undisturbed photosphere.

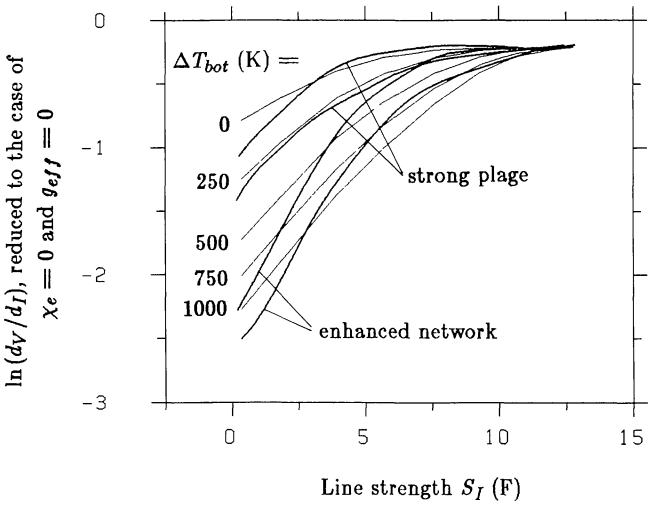

Fig. 10. $\ln(d_V/d_I)$ vs. S_I. The thick curves represent smoothed averages (cubic splines) of the data, reduced to the case that $\chi_e=0$ and $g_{\rm eff}=0$. The two steeper curves correspond to enhanced network elements, the other two are from plage data. The thin lines have been calculated using models with $\Delta T_{\rm top}=500$ K and (in the order of increasing steepness of the curves) $\Delta T_{\rm bot}=0$, 250, 500, 750, and 1000 K. The empirical curves have been shifted such that they coincide at the S_I of the strongest lines

5.2. *Magnetic field strengths and filling factors*

Table 2 is a compilation of the magnetic field strengths and filling factors (near $\tau_{5000}=1$) of the five observed regions. The magnetic field strength B has first been determined from regression coefficient x_5 using (3.3), and from coefficient x_6 using (3.6) with $\alpha=0$ (columns 2 and 3). The use of $\alpha=0$ in (3.6) corresponds to the assumption that the Stokes I profiles are unaffected by the magnetic component). Almost all information on the field strength magnetic component). Almost all information on the fieldstrength is contained in the I_V profiles, derived from Stokes V. The averages of the derived values of B have then been corrected through multiplication by $(1-\alpha)^{-1/2}$ assuming $\delta=1/3$ (a value suggested by our model calculations), and using α values determined as

Table 2. Comparison between the field strengths in network and plages, derived from regression coefficients assuming the Zeeman splitting to be small (see text)

Type of region	B_{x_5} (G) from (3.3) for $\alpha=0$	B_{x_6} (G) from (3.6) for $\alpha=0$	Average B_x (G) corrected for α	Estimated α (%)
Network	1700	1690	1720	3.0 ± 1.5
Network	1230	1490	1390	4.0 ± 2.0
Weak plage	1540	1320	1465	5.0 ± 2.5
Strong plage	1260	1560	1515	13.3 ± 6.7
Strong plage	1460	1540	1625	14.7 ± 7.4

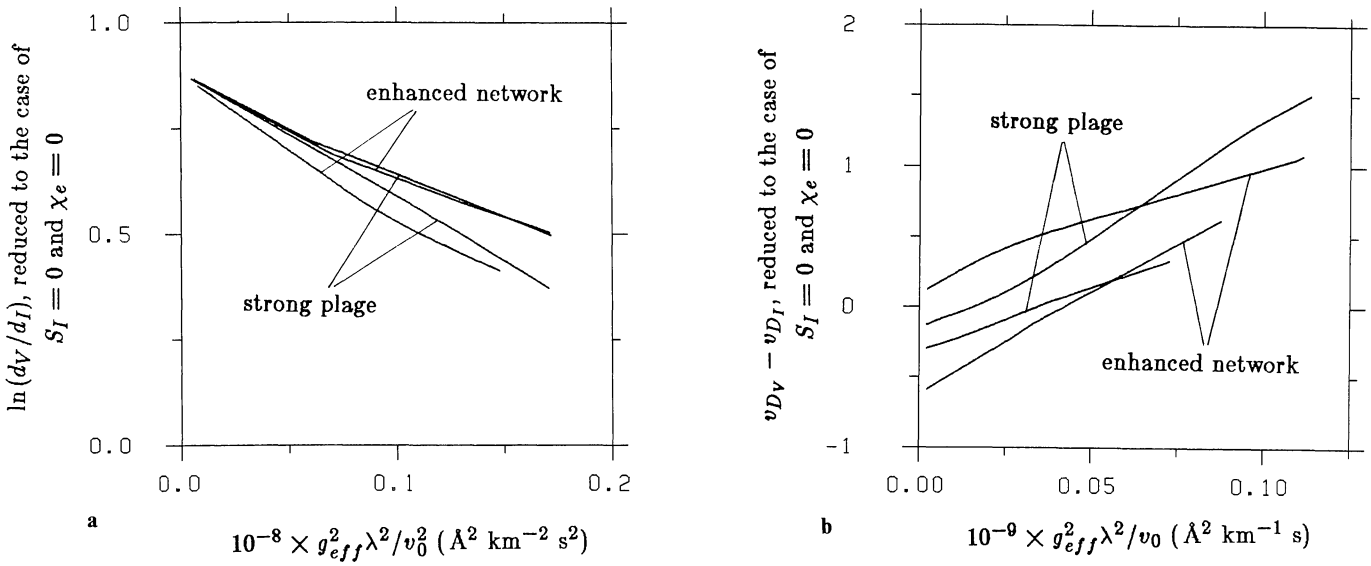

Fig. 11. a Smoothed averages of $\ln(d_V/d_I)$ vs. $g_{\text{eff}}^2\lambda^2/v_0^2$, reduced to the case that $S_I=0$ and $\chi_e=0$, for two network and two plage regions. Note the approximately equal gradient of all four curves. The curves of the two plages have been shifted vertically in order to facilitate comparison. **b** Smoothed averages of $v_{D_V}-v_{D_I}$ vs. $g_{\text{eff}}^2\lambda^2/v_0$, reduced to the case that $S_I=0$ and $\chi_e=0$, for the same regions as in **a**. The curves are all unshifted

described below (column 5). No significant difference between the field strengths in the network and in plages can be seen. These field-strength values are considerably larger than the values obtained by comparing model calculations with the observed $v_{D_V}-v_{D_I}$ vs. $g_{\text{eff}}^2\lambda^2/v_0$ and $\ln(d_V/d_I)$ vs. $g_{\text{eff}}^2\lambda^2/v_0^2$ curves, which gives values around 1 kG (Fig. 9), consistent with the results obtained with the line ratio technique (Stenflo, 1973). This relatively large difference in field strengths stems from the fact that (3.3) and (3.6) are only valid when the Zeeman splitting of a line is much smaller than its Doppler width. This approximation breaks down for narrow lines with large Zeeman splitting in the presence of kG fields, since the higher order terms in the Taylor expansion (2.1) then become important. This is demonstrated by the theoretical curves in Fig. 9, which are not straight lines as functions of $g_{\text{eff}}^2\lambda^2/v_0$ and $g_{\text{eff}}^2\lambda^2/v_0^2$ as they would be if only the first two terms of (2.1) were of importance.

As the field strengths in Table 2 are based on the invalid assumption of small Zeeman splitting, they should not be quoted as the actual fluxtube field strengths. To determine the actual field strength the model fits illustrated in Fig. 9, or the line-ratio technique are the appropriate methods to use. The purpose of Table 2 is to show that the Zeeman broadening and saturation are the same in plages and the network, indicating the same actual field strength in these different structures. This conclusion of equal field strength is also supported by Fig. 11.

All these results represent lower limits for the field strength amplitude, since we have assumed a rectangular magnetic field cross section of the fluxtubes.

Magnetic filling factors, α, can be determined in a model dependent manner from the $\ln(d_V/d_I)$ vs. S_I diagram and the magnetic field strength. The α values thus determined are lower limits, since any depolarization in the telescope reduces the height of the V profiles and, therefore, the derived value of α. Stenflo and Harvey (1984) have suggested that there is also a still unexplained calibration error of a factor of two in all the polarization data. In Table 2, column 5, we have included α values determined using models with $\Delta T_{\text{top}}=500$ K, multiplied by a factor of two to correct for the presumed calibration error. Models with lower ΔT_{top} give smaller values of α. These differences are, however, insignificant compared with the observational uncertainty in α. Our estimated values of α in column 5 have been used to obtain the B_x values in column 4. Fortunately, the influence of α on the derived values of B_x in Table 2 is not very large.

5.3. *Velocities and microturbulence*

Due to the difference in $\langle B\rangle$ between the network and the plages, which leads to a difference in amplitude of the V profiles, it is impossible to compare the absolute asymmetries of the active and quiet regions without prior knowledge of the average magnetic field. The relative asymmetries, however, are on the same scale and can accordingly be compared easily. The asymmetry turns out to be surprisingly similar for the plage and network regions as shown by Fig. 12. The relative area asymmetries are identical within the scatter of the points. The relative amplitude asymmetry is slightly smaller for the plage, although the scatter is quite large. The velocity structure in both types of regions should therefore be very similar. The slightly smaller amplitude asymmetry in the plages may be a result of the larger area factor, since the magnetic fields from surrounding fluxtubes prevent the fluxtube cross sections from increasing rapidly with height, thus keeping the vertical magnetic field gradient smaller. A gradient along the line of sight is needed to produce a Stokes V asymmetry (Auer and Heasley, 1978). At disk center, where our observations were made, the line of sight coincides with the vertical direction.

We have checked that our observed asymmetries are not caused by instrumental effects and really represent fluxtube physics on the sun. Thus for instance the polarity of the observed magnetic field does not affect the behavior of the Stokes V asymmetry described by Fig. 12. The predominance of the amplitude and area of the blue-wing Stokes V peak over the peak in the red wing applies to both positive and negative polarity regions. This excludes the possibility that the instrument somehow would favour one sense of circular polarization over the other sense. Further, the absence of any wavelength dependence of the Stokes V asymmetries suggests that the effects of differential chromatic

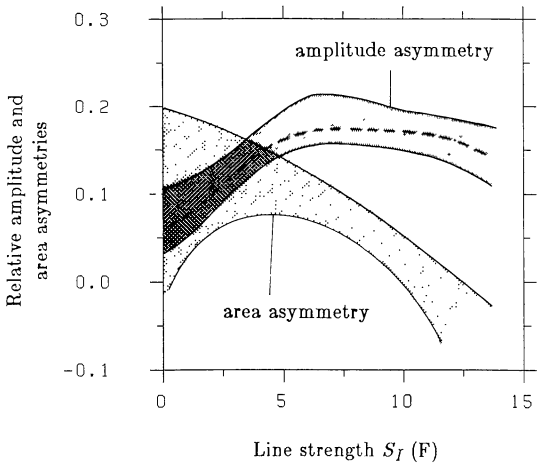

Fig. 12. The shaded areas are bounded by the envelopes of the smoothed relative amplitude (dark shading) and area (light shading) asymmetry curves of all the observed regions, plotted vs. S_I. The dashed line running between the amplitude asymmetry envelopes is a boundary between the curves of the plage and network regions. The smoothed plage curves lie below this line whereas the network curves lie above it. No such distinction can be made for the area asymmetry

properties of any of the optical elements have not infiltrated our results.

For Fe I lines around 5200 Å the same Stokes V asymmetries were found with the vertical grating spectrometer of the McMath telescope (Stenflo and Harvey, 1984), with which a much larger number of magnetic regions could be sampled. The results do not depend on the time of day, and are thus uncorrelated with the position of the obliquely reflecting heliostat mirror.

As pointed out in Sect. 3, the shapes of the area and amplitude asymmetry curves are quite different, as shown in Figs. 6 and 12. This is consistent with the suggestion that different mechanisms are responsible for producing the area and amplitude asymmetries. The amplitude asymmetry of any one particular line depends only on the maximum V amplitudes and is, therefore, sensitive to only a limited height range, whereas the area asymmetry, being an integral quantity, is sensitive to a much larger range of heights.

The relation between the observed Stokes V asymmetry and the underlying velocity structure is very complex. As a matter of fact we tend to believe that no models with stationary flows are adequate, since the models that are able to reproduce the Stokes V asymmetries also give rise to large net Doppler shifts of the zero-crossing point of the Stokes V profile, contrary to observations (Stenflo and Harvey, 1984). One conceivable non-stationary flow with zero net Doppler shift is represented by fluxtube oscillations. The integration in time and space over an ensemble of fluxtubes in various phases of their dynamics, which is represented by our observations, may then give rise to the asymmetries. In the present paper we restrict ourselves to present the observational data that may serve to constrain future modelling, and leave the interpretation for a later investigation.

The microturbulence velocity inside the fluxtube can only be determined very approximately. Our data indicate values between 0.5 and 1 times the photospheric ξ_t.

6. Conclusions

In the present work some preliminary results on the physical properties of small photospheric fluxtubes have been presented. Using statistical methods it has been possible to partially separate the effects of different physical conditions in the fluxtubes on the line parameters. Using very simple model calculations some constraints on fluxtube properties could be set. The temperature structure of fluxtubes in plages and in quiet sun network elements was found to be different, in contrast to the results of some earlier authors. This difference cannot be explained by the different magnetic filling factors found in the two types of regions. The data can be reproduced by preliminary model calculations having a temperature enhancement of between 200 and 500 K at the $\tau_{5000}=10^{-4}$ level for both the plage and network, whereas the temperature enhancement at $\tau_{5000}=1$ needed is around 400–600 K for the network, and around 100 K for the plage.

Due to the excellent spectral resolution and the large number of lines studied, it has been possible to determine the intrinsic field strength in the fluxtubes, B, directly from the line broadening, using lines lying in the visible part of the spectrum [in contrast to Harvey and Hall (1975), who used a carefully selected line in the infrared], as well as from the decrease in line depth due to Zeeman saturation. The kG field strengths have been confirmed, as have the results that plages and the network have about the same field strengths at the photospheric level.

We have also been able to present quantitative data on the asymmetries of the Stokes V profiles. These data suggest that the velocity gradient changes considerably with height. Plages and the network show little difference in their asymmetry variations as a function of line strength, indicating a similarity between their velocity structures.

The determination of the average magnetic field strength $\langle B \rangle$ or area factor α depends on a correct determination of the amount of temperature weakening of the lines. Since all Fe I lines are substantially temperature weakened, there remains some uncertainty as to where the zero point of the line weakening on the ΔT scale is. It would therefore be of particular interest to perform a similar study as the present one for a set of Fe II lines, since they are much less temperature sensitive.

To reach to chromospheric levels in the fluxtubes, strong lines which must be treated with non-LTE theory have to be used. It was indicated in Stenflo et al. (1984) that the Mg I b_2 line could be particularly useful for this purpose.

However, even the description of the photospheric part of the fluxtube will require a substantially more sophisticated fluxtube model than the one used in the present paper, which only served as an exploratory tool to study the information contents of the various scatter plots. In a self-consistent fluxtube model the magnetic field divergence and stresses, horizontal pressure balance and the velocity field have to be properly accounted for. Although the construction of empirical fluxtube models is a very complex problem, it can now be approached in a more systematic way using the new observational foundations of our FTS data.

Acknowledgements. We are grateful to J. W. Harvey and J. W. Brault for their support and collaboration in obtaining the FTS data used in the present paper. The work of one of us (S.K.S.) was supported by grants No. 2.084-0.81 and 2.814-0.83 from the Swiss National Science Foundation, which is gratefully acknowledged.

References

Allen, C.W.: 1973, Astrophysical Quantities, Athlone Press, London

Auer, L.H., Heasley, J.N.: 1978, *Astron. Astrophys.* **64**, 67

Baschek, B., Scholz, M.: 1982, in *Landolt-Börnstein, New Series* **VI/2b**, 91, Springer Verlag, Berlin
Beckers, J.M.: 1969a, *Solar Phys.* **9**, 372
Beckers, J.M.: 1969b, *Solar Phys.* **10**, 262
Brault, J.W.: 1978, in *Proc.* JOSO *Workshop "Future Solar Optical Observations – Needs and Constraints"*, eds. G. Godoli, G. Noci, A. Righini, *Osserv. Mem. Oss. Astrofis. Arcetri* **106**, 33
Chapman, G.A.: 1977, *Astrophys. J. Suppl.* **33**, 35
Chapman, G.A.: 1979, *Astrophys. J.* **232**, 923
Cook, J.W., Brueckner, G.E., Bartoe, J.-D.F.: 1983, *Astrophys. J.* **270**, L89
Deinzer, W., Hensler, G., Schmitt, D., Schüssler, M., Weisshaar, E.: 1982, in *Solar and Stellar Magnetic Fields: Origins and Coronal Effects*, ed. J. O. Stenflo, IAU *Symp.* **102**, 67
Frazier, E.N., Stenflo, J.O.: 1972, *Solar Phys.* **27**, 330
Frazier, E.N., Stenflo, J.O.: 1978, *Astron. Astrophys.* **70**, 789
Gingerich, O., Noyes, R.W., Kalkofen, W., Cuny, Y.: 1971, *Solar Phys.* **18**, 347
Giovanelli, R.G.: 1980, *Solar Phys.* **68**, 49
Gough, D.O., Taylor, R.J.: 1966, *Monthly Notices Roy. Astron. Soc.* **133**, 85
Gurtovenko, E.A.: 1975, *Solar Phys.* **45**, 25
Harvey, J.W., Hall, D.: 1975, *Bull. Am. Astron. Soc.* **7**, 459
Holweger, H.: 1973, *Solar Phys.* **30**, 35
Koutchmy, S., Stellmacher, G.: 1978, *Astron. Astrophys.* **67**, 93
Landi Degl'Innocenti, E.: 1982, *Solar Phys.* **77**, 285
Lites, B.W.: 1972, NCAR Cooperative Thesis No. 28, NCAR, Boulder, Colorado
Osherovich, V.A., Flå, T., Chapman, G.A.: 1983, *Astrophys. J.* **286**, 412
Ribes, E., Semel, M.: 1980, in *Proc. Japan-France Seminar on Solar Physics*, eds. F. Moriyama, J. C. Henoux, p. 129
Shine, R.A., Linsky, J.L.: 1974, *Solar Phys.* **37**, 145
Simon, G.W., Zirker, J.B.: 1974, *Solar Phys.* **35**, 331
Spruit, H.C.: 1974, *Solar Phys.* **34**, 277
Spruit, H.C.: 1976, *Solar Phys.* **50**, 269
Stellmacher, G., Wiehr, E.: 1979, *Astron. Astrophys.* **75**, 263
Stenflo, J.O.: 1973, *Solar Phys.* **32**, 41
Stenflo, J.O.: 1975, *Solar Phys.* **42**, 79
Stenflo, J.O.: 1976, in *Basic Mechanisms of Solar Activity*, eds. V. Bumba, J. Kleczek, IAU *Symp.* **71**, 69
Stenflo, J.O., Lindegren, L.: 1977, *Astron. Astrophys.* **59**, 367
Stenflo, J.O., Harvey, J.W., Brault, J.W., Solanki, S.K.: 1984, *Astron. Astrophys.* **131**, 333
Stenflo, J.O., Harvey, J.W.: 1984, *Solar Phys.* (in press)
Unno, W., Ribes, E.: 1979, *Astron. Astrophys.* **73**, 314
Unsöld, A.: 1968, Physik der Sternatmosphären, Springer Verlag, Berlin